

# Characterization of nighttime formation of particulate organic nitrates based on high-resolution aerosol mass spectrometry in an urban atmosphere in China

Kuangyou Yu<sup>1,2,\*</sup>, Qiao Zhu<sup>1,\*</sup>, Ke Du<sup>2</sup>, Xiao-Feng Huang<sup>1</sup>

<sup>1</sup>Key Laboratory for Urban Habitat Environmental Science and Technology, School of Environment and Energy, Peking University Shenzhen Graduate School, Shenzhen, 518055, China.

<sup>2</sup>Department of Mechanical and Manufacturing Engineering, University of Calgary, Calgary, Canada.

\* Authors have equal contribution.

**Abstract.** Organic nitrates are important atmospheric species that significantly affect the cycling of NO<sub>x</sub> and ozone production. However, characterization of particulate organic nitrates and their sources in polluted atmosphere is a big challenge and has been little performed in Asia. In this study, an Aerodyne high-resolution time-of-flight aerosol mass spectrometer (HR-ToF-AMS) was deployed at an urban site in China from 2015 to 2016 to characterize particulate organic nitrates in total nitrates with high time resolution. Based on cross validation of two different data processing methods, organic nitrates were effectively quantified to contribute a notable fraction of organic aerosol (OA): 9-21% in spring, 11-25% in summer and 9-20% in autumn; while organic nitrates were found to little exist in winter. The good correlation between organic nitrates and fresh secondary organic aerosol (SOA) at night as well as the diurnal trend of size distribution of organic nitrates indicated a key role of nighttime secondary formation in Shenzhen, which is consistent with what found in the US and Europe. The size distribution of organic nitrates also implied that organic nitrates were mainly a local product and could have strong removal during air mass transport. Furthermore, theoretical calculations of nighttime SOA production of NO<sub>3</sub> reactions with volatile organic compounds (VOCs) measured during the spring campaign were performed, resulting in two biogenic VOCs ( $\alpha$ -pinene and limonene) and one anthropogenic VOC (styrene) identified as the key VOC precursors for particulate organic nitrates. The comparison with similar studies in the literature implied that nighttime particulate organic nitrates formation could be NO<sub>x</sub>-controlled. This study proposes that different from the previous cases in the United States and Europe, modeling nighttime particulate organic nitrate formation should incorporate not only biogenic VOCs but also anthropogenic VOCs with high SOA yield for urban air pollution in China, which call for relevant smog chamber studies to support in future.

---

Correspondence to: X.-F. Huang ([huangxf@pku.edu.cn](mailto:huangxf@pku.edu.cn))

## 30 1. Introduction

31 Organic nitrates (ON) in aerosols have an important impact on the fate of NO<sub>x</sub> and ozone production (Lelieveld et al., 2016),  
32 which can be formed in a minor channel of the reaction between peroxy radicals and NO (R1 and R2) (usually, an increased  
33 fraction of this reaction leads to the formation of alkoxy radicals and NO<sub>2</sub> (R3)) or via the NO<sub>3</sub>-induced oxidation of unsaturated  
34 hydrocarbons (R4). Even though some recent studies have suggested that the formation of organic nitrates from peroxy radicals  
35 and NO may play a larger role than previously recognized (Teng et al., 2015, 2017), yields of organic nitrates via NO<sub>3</sub> reacting  
36 with alkenes are generally much higher (Fry et al., 2009; Ayres et al., 2015; Boyd et al., 2015, 2017).



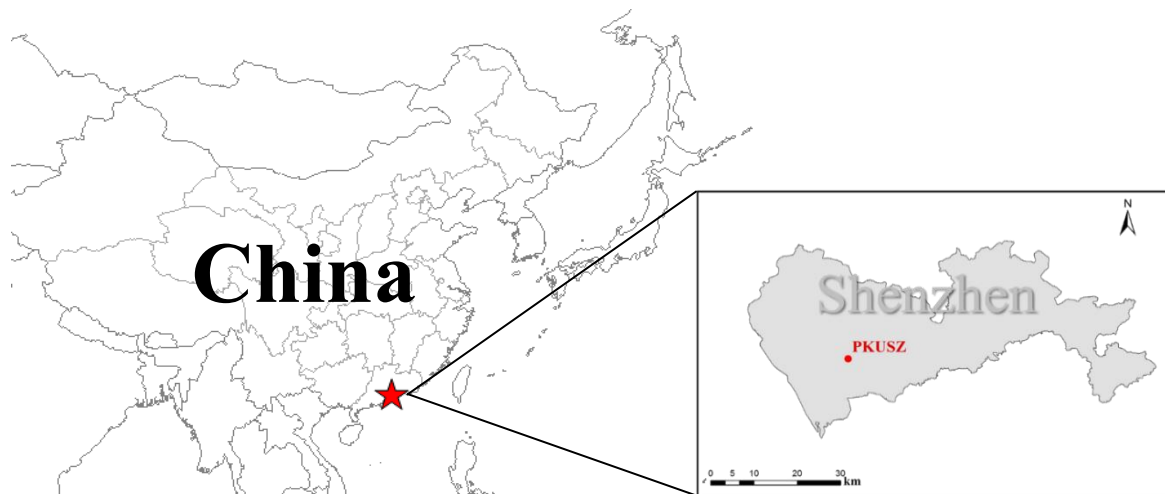
41 Several direct methods have been developed to measure total organic nitrates (gas + particle) in the real atmosphere. For  
42 example, Rollins et al. (2012) used a thermal-dissociation laser-induced fluorescence technique (TD-LIF) to observe organic  
43 nitrates in the United States; Sobanski et al. (2017) measured organic nitrates in Germany using the thermal dissociation cavity  
44 ring-down spectroscopy (TD-CRDS). Field and laboratory studies around the world indicated that particulate organic nitrates  
45 could contribute a large portion of secondary organic aerosol (SOA) (Rollins et al., 2012; Xu et al., 2015a; Fry et al., 2013;  
46 Ayres et al., 2015; Boyd et al., 2015; Lee et al., 2016). Recently, researchers have proposed some estimation methods for  
47 particle-phase organic nitrates based on aerosol mass spectrometry (AMS) with high time resolution (Farmer et al., 2010; Hao  
48 et al., 2014; Xu et al., 2015a, 2015b). Ng et al. (2017) reviewed the nitrate radical chemistry and the abundance of particulate  
49 organic nitrates in the United States and Europe, and further concluded that particulate organic nitrates are formed substantially  
50 via NO<sub>3</sub>+BVOC chemistry, which plays an important role in SOA formation. Unfortunately, relevant Chinese datasets are  
51 scarce yet and not included in this review. This was because (1) the contributions of organic nitrates in SOA and total nitrates  
52 in Chinese atmosphere remain poorly understood; (2) the anthropogenic and biogenic precursor emissions in China are largely  
53 different from those in the United States and Europe, and thus cannot be easily estimated. To our best knowledge, few studies  
54 have investigated the concentrations and formation pathways of particulate organic nitrates in China. Xu et al. (2017) estimated  
55 the mass concentration of organic nitrogen in Beijing using AMS, but in this study they ignored the contribution of NO<sub>x</sub><sup>+</sup>  
56 family, which are the major fragments of organic nitrates.

57 Shenzhen is a megacity of China in a subtropical region, where photochemical reactions are very active with high NO<sub>x</sub> and  
58 both biogenic and anthropogenic VOC emissions (Zhang et al., 2008). To assess the evolution of particulate organic nitrates  
59 in a polluted urban atmosphere, we deployed an Aerodyne high-resolution time-of-flight aerosol mass spectrometer (HR-ToF-  
60 AMS) and other instruments in Shenzhen from 2015 to 2016 in this study. Organic nitrates and their contributions to OA in  
61 different seasons were estimated by different methods using the HR-ToF-AMS datasets obtained, based on which, the  
62 secondary formation pathway of particulate organic nitrates in Shenzhen was further explored.

63 **2. Experiment methods**

64 **2.1 Sampling site and period**

65 The sampling site (22.6°N, 113.9°E) was on the roof (20 m above ground) of an academic building on the campus of Peking  
66 University Shenzhen Graduate School (PKUSZ), which is located in the western urban area in Shenzhen (Figure 1). This site  
67 is mostly surrounded by subtropical plants without significant anthropogenic emission sources nearby, except a local road  
68 ~100 m from the site. In this study, we used the statistical data from the Meteorological Bureau of Shenzhen Municipality  
69 (<http://www.szmb.gov.cn/site/szmb/Esztq/index.html>) as the reference data to determine the sampling periods for four  
70 different seasons during 2015-2016, as shown in Table 1.



71

72

**Figure 1.**The location of the sampling site.

73 **Table 1.**Meteorological conditions, PM<sub>1</sub> species concentrations and relevant parameters for different sampling periods in  
74 Shenzhen.

	Sampling period	4.1-4.30, 2016	8.1-8.31, 2015	11.4-11.30, 2015	1.21-2.3, 2016
		Spring	Summer	Autumn	Winter
<b>Meteorology</b>	T (°C)	24.5±2.5	29.0±3.0	23.6±3.7	10.7±4.7
	RH (%)	78.0±12.7	71.2±17.5	68.2±15.8	75.4±18.7
	WS (m s <sup>-1</sup> )	1.4±0.8	1.0±0.7	1.2±0.7	1.5±0.8
<b>Species</b>	Org	4.3±3.2	10.0±6.9	7.8±5.9	5.1±3.5
	SO <sub>4</sub> <sup>2-</sup>	3.2±1.8	5.8±3.3	2.3±1.5	1.9±1.2
	Total NO <sub>3</sub> <sup>-</sup>	0.96±1.4	0.91±0.90	1.3±1.4	1.6±1.0

$(\mu\text{g m}^{-3})$	$\text{NH}_4^+$	1.4±0.8	2.0±1.1	1.1±0.8	1.2±0.6
	$\text{Cl}^-$	0.14±0.19	0.03±0.05	0.22±0.36	0.64±0.85
	BC	1.9±2.1	2.4±1.6	3.5±2.6	2.4±1.5
	Total	12.0±8.9	15.1±13.8	11.8±9.5	12.2±7.2
<b>ON relevant</b>	$R_{\text{NH}_4\text{NO}_3}$	2.80	3.20	3.32	3.48
	$R_{\text{obs}}$	3.74	6.14	4.30	3.55
<b>parameters</b>	Fraction of positive numbers of $R_{\text{obs}} - R_{\text{NH}_4\text{NO}_3}$	99%	99%	84%	47%

## 75 2.2 Instrumentation

### 76 2.2.1 High Resolution Time-of-Flight Aerosol Mass Spectrometer

77 During the sampling periods, chemical composition of non-refractory  $\text{PM}_{10}$  was measured by an Aerodyne HR-ToF-AMS, and  
78 detailed descriptions of this instrument are given in the literature (DeCarlo et al., 2006; Canagaratna et al., 2007). The setup  
79 and operation of the HR-ToF-AMS can be found in our previous publications (Huang et al., 2010, 2012; Zhu et al., 2016). To  
80 remove coarse particles, a  $\text{PM}_{2.5}$  cyclone inlet was installed before the sampling copper tube with a flow rate of  $10 \text{ l min}^{-1}$ .  
81 Before entering the AMS, the sampled air was dried by a nafion dryer (MD-070-12S-4, Perma Pure Inc.) to eliminate the  
82 potential influence of relative humidity on particle collection (Matthew et al., 2008). The ionization efficiency (IE) calibrations  
83 were performed using pure ammonium nitrate every two weeks. The relative ionization efficiencies (RIEs) used in this study  
84 were 1.2 for sulfate, 1.1 for nitrate, 1.3 for chloride, 1.4 for organics and 4.0 for ammonium, respectively (Jimenez et al., 2003).  
85 Composition-dependent collection efficiencies (CEs) were applied to the data according to the method in Middlebrook et al.  
86 (2012). The instrument was operated at two ion optical modes with a cycle of 4 min, including 2 min for the mass-sensitive  
87 V-mode and 2 min for the high mass resolution W-mode. The HR-ToF-AMS data analysis was performed using the software  
88 SQUIRREL (version 1.57) and PIKA (version 1.16) written in Igor Pro 6.37 (Wave Metrics Inc.)  
89 (<http://cires1.colorado.edu/jimenezgroup/ToFAMSResources/ToFSoftware/index.html>).

### 90 2.2.2 Other co-located instruments

91 In addition to the HR-ToF-AMS, other relevant instruments were deployed at the same sampling site. An aethalometer (AE-  
92 31, Magee) was used for measurement of refractory black carbon (BC) with a resolution of 5 min. An SMPS system (3775  
93 CPC and 3080 DMA, TSI Inc.) was used to obtain the particle number size distribution in 15–615 nm (mobility diameter) with  
94 a time resolution of 5 min. Ozone and  $\text{NO}_x$  were measured by a 49i ozone analyzer and a 42i nitrogen oxide analyzer (Thermo  
95 Scientific), respectively. In the spring campaign, ambient VOC concentrations were also measured using an on-line VOC  
96 monitoring system (TH-300B, Tianhong Corp.), including an ultralow-temperature preconcentration cold trap and an

97 automated in-situ gas chromatograph (Agilent 7820A) equipped with a mass spectrometer (Agilent 5977E). The system had  
 98 both a flame ionization detector (FID) gas channel for C2–C5 hydrocarbons and a mass spectrometer (MS) gas channel for  
 99 C5–C12 hydrocarbons, halohydrocarbons and oxygenated VOCs. A complete working cycle of the system was one hour and  
 100 included five steps: sample collection, freeze-trapping, thermal desorption, GC-FID/MS analysis, heating and anti-blowing  
 101 purification. The sample collection time was 5 min, the sampling flow was 60 ml min<sup>-1</sup>, and the anti-blowing flow was 200 ml  
 102 min<sup>-1</sup>. The calibration of over 100 VOCs was performed using mixed standard gas before and after the campaign. Detection  
 103 limits for most compounds were near 5 pptv. More description of this instrument can be found in Wang et al. (2014).

### 104 **2.3 Organic nitrate estimation methods**

105 In this study, we used two independent methods to estimate particulate organic nitrates based on the AMS data, following the  
 106 approaches in Xu et al. (2015b). The first method is based on the NO<sup>+</sup>/NO<sub>2</sub><sup>+</sup> ratio (NO<sub>X</sub><sup>+</sup> ratio) in the HR-AMS spectrum. Due  
 107 to the very different NO<sub>X</sub><sup>+</sup> ratios of organic nitrates and inorganic nitrate (i.e., R<sub>ON</sub> and R<sub>NH<sub>4</sub>NO<sub>3</sub></sub>, respectively) (Farmer et al.,  
 108 2010; Boyd et al., 2015; Fry et al., 2008; Bruns et al., 2010), the NO<sub>2</sub><sup>+</sup> and NO<sup>+</sup> concentrations of organic nitrates (NO<sub>2,ON</sub> and  
 109 NO<sub>ON</sub>) can be quantified with the HR-AMS data via Eqs. (1) and (2), respectively (Farmer et al., 2010):

$$110 \quad NO_{2,ON}^+ = \frac{NO_{2,obs}^+ \times (R_{obs} - R_{NH_4NO_3})}{R_{ON} - R_{NH_4NO_3}} \quad (1)$$

$$111 \quad NO_{ON}^+ = R_{ON} \times NO_{2,ON} \quad (2)$$

112 where R<sub>obs</sub> is the NO<sub>X</sub><sup>+</sup> ratio from the observation. The value of R<sub>ON</sub> is difficult to determine because it varies between  
 113 instruments and precursor VOCs. However, R<sub>NH<sub>4</sub>NO<sub>3</sub></sub> was determined by IE calibration using pure NH<sub>4</sub>NO<sub>3</sub> every two weeks  
 114 for each campaign and the results showed stable values: In spring, the average R<sub>NH<sub>4</sub>NO<sub>3</sub></sub> was 2.66 for the first IE calibration and  
 115 2.94 for the second one; in summer, the average R<sub>NH<sub>4</sub>NO<sub>3</sub></sub> was 3.05 and 3.34 for the first and second IE calibrations, respectively;  
 116 in autumn, the average R<sub>NH<sub>4</sub>NO<sub>3</sub></sub> was 3.33 and 3.31 for the first and second IE calibrations, respectively; in winter, the average  
 117 R<sub>NH<sub>4</sub>NO<sub>3</sub></sub> was 3.45 and 3.51 for the first and second IE calibrations, respectively. We adopted the R<sub>ON</sub>/R<sub>NH<sub>4</sub>NO<sub>3</sub></sub> estimation range  
 118 (from 2.08 to 3.99) for variation of precursor VOCs in the literature to determine R<sub>ON</sub> (Farmer et al., 2010; Boyd et al., 2015;  
 119 Bruns et al., 2010; Sato et al., 2010; Xu et al., 2015b), and thus two R<sub>ON</sub> values were calculated for each season to provide the  
 120 upper bound (NO<sub>3\_org\_ratio\_1</sub>) and lower bound (NO<sub>3\_org\_ratio\_2</sub>) of NO<sub>3,org</sub> mass concentration.

121 The second method is based on the traditional positive matrix factorization (PMF) analysis of HR organic mass spectra for  
 122 resolving different organic factors (Zhang et al., 2011; Ng et al., 2010; Huang et al., 2013), and the same analysis of HR organic  
 123 mass spectra, but combined with NO<sup>+</sup> and NO<sub>2</sub><sup>+</sup> ions, was performed to separate NO<sup>+</sup> and NO<sub>2</sub><sup>+</sup> ions into different organic  
 124 factors and an inorganic nitrate factor (Hao et al., 2014; Xu et al., 2015b). The PMF analysis procedures in this study can be  
 125 found in our previous publications (Huang et al., 2010; Zhu et al., 2016; He et al., 2011), resulting in three organic factors and  
 126 one inorganic factor in spring, summer and autumn: a hydrocarbon-like OA (HOA) characterized by C<sub>n</sub>H<sub>2n+1</sub><sup>+</sup> and C<sub>n</sub>H<sub>2n-1</sub><sup>+</sup> and  
 127 O/C of 0.11 to 0.18, a less-oxidized oxygenated OA (LO-OOA) characterized by C<sub>x</sub>H<sub>y</sub>O<sub>z</sub><sup>+</sup> especially C<sub>2</sub>H<sub>3</sub>O<sup>+</sup> and O/C of 0.28  
 128 to 0.70, a more-oxidized oxygenated OA (MO-OOA) also characterized by C<sub>x</sub>H<sub>y</sub>O<sub>z</sub><sup>+</sup> especially CO<sub>2</sub><sup>+</sup> and O/C of 0.78 to 1.24,

129 and a nitrate inorganic aerosol (NIA) characterized by overwhelming  $\text{NO}^+$  and  $\text{NO}_2^+$ , as indicated in Fig S6. According to the  
130 diagnostic plots of the PMF analysis shown in Figure S2 to S4, the same organic factors as those in the traditional PMF analysis  
131 of only organic mass spectra were indeed obtained. The  $\text{NO}^+$  and  $\text{NO}_2^+$  ions were distributed among different OA factors and  
132 the NIA factor; thus the concentrations of nitrate functionality ( $\text{NO}_{org}^+$  and  $\text{NO}_{2,org}^+$ ) in organic nitrates ( $\text{NO}_{3,org}$ ) are equal to  
133 the sum of  $\text{NO}_2^+$  and  $\text{NO}^+$  via Eqs. (3) and (4), respectively (Xu et al., 2015b):

$$134 \quad \text{NO}_{2,org}^+ = \sum([\text{OA factor}]_i \times f_{\text{NO}_2,i}) \quad (3)$$

$$135 \quad \text{NO}_{org}^+ = \sum([\text{OA factor}]_i \times f_{\text{NO},i}) \quad (4)$$

136 where  $[\text{OA factor}]_i$  represents the mass concentration of OA factor  $i$ , and  $f_{\text{NO}_2,i}$  and  $f_{\text{NO},i}$  represent the mass fractions of  $\text{NO}_2^+$   
137 and  $\text{NO}^+$ , respectively.

138 It should be noted that although the 4-factor solution seemed to have a “mixed factor” problem to some extent (Zhu et al.,  
139 2018), such as HOA mixed with COA (clear  $\text{C}_3\text{H}_3\text{O}^+$  in  $m/z$  55 for spring, summer and autumn) (Mohr et al., 2012) and BBOA  
140 mixed with LO-OOA (clear  $m/z$  60 and 73 signals in LO-OOA in autumn) (Cubison et al., 2011), running PMF with more  
141 factors would produce unexplained factors but little influence the apportion of  $\text{NO}^+$  and  $\text{NO}_2^+$  ions between organic nitrates  
142 and inorganic nitrate (Table S1). In addition, the uncertainties of  $\text{NO}^+$  and  $\text{NO}_2^+$  ions in the OA factors across different peak  
143 values (from  $-1.0$  to  $1.0$ ) were very small (Table S2). Therefore, the 4-factor solution was finally used for quantifying organic  
144 nitrates in spring, summer and autumn.

### 145 **3. Results and discussion**

#### 146 **3.1 Organic nitrate estimation**

147 Table 2 shows the concentrations of nitrate functionality in organic nitrates (i.e.,  $\text{NO}_{3,org}$ ), estimated by both the  $\text{NO}^+/\text{NO}_2^+$   
148 ratio method and PMF method, and their contributions to the total measured nitrate. It should be noted that the small difference  
149 between the average  $R_{\text{obs}}$  and  $R_{\text{NH}_4\text{NO}_3}$  in winter leads to a large portion of negative data using the  $\text{NO}^+/\text{NO}_2^+$  ratio method  
150 (Table 1), and the result from the PMF method shows the contribution of organic nitrates in total nitrates is only 4.2% in winter  
151 (Figure S6), suggesting a negligible contribution of organic nitrates. Thus, we will only discuss organic nitrate estimation  
152 results in spring, summer and autumn. No matter by the  $\text{NO}^+/\text{NO}_2^+$  ratio method or by the PMF method, organic nitrates had  
153 the highest ambient concentration ( $0.34\text{-}0.53 \mu\text{g m}^{-3}$ ) and proportion in total nitrates (41-64%) in summer among the different  
154 seasons, which is consistent with the finding in the literature (Ng et al., 2017) and presents a different seasonal trend in  
155 comparison with that of total nitrates in Table 1. Assuming the average molecular weight of organic nitrates of 200 to 300 g  
156  $\text{mol}^{-1}$  (Rollins et al., 2012), we found that organic nitrates contributed 9-21% to OA in spring, 11-25% in summer and 9-20%  
157 in autumn.

158 In the PMF method, the mass fractions of organic nitrates in HOA, LO-OOA and MO-OOA were 31%, 49% and 20%,  
159 respectively, in spring; 28%, 52% and 20%, respectively, in summer; 30%, 46% and 24%, respectively, in autumn. The major

160 fraction of organic nitrates occurring in LO-OOA for the three seasons implied that organic nitrates were mostly related to  
 161 fresher secondary OA formation. The NIA factor in all seasons was dominated by  $\text{NO}^+$  and  $\text{NO}_2^+$ , but also contained some  
 162 organic fragments, such as  $\text{CO}_2^+$  and  $\text{C}_2\text{H}_3\text{O}^+$ , which agreed with the findings in the literature (Hao et al., 2014; Xu et al.,  
 163 2015b; Sun et al., 2012) and indicated potential interference of organics in the NIA factor. Also note that the  $\text{NO}^+/\text{NO}_2^+$  ratios  
 164 in NIA (2.93 for spring, 3.53 for summer and 3.54 for autumn) were higher than that for pure  $\text{NH}_4\text{NO}_3$  (Table 1), indicating  
 165 an underestimation of  $\text{NO}_{3,\text{org}}$  concentration by the PMF method. This may also explain why the concentration of  $\text{NO}_{3,\text{org}}$   
 166 estimated using the PMF method was always close to the lower estimation bound of  $\text{NO}_{3,\text{org}}$  concentration using the  $\text{NO}^+/\text{NO}_2^+$   
 167 ratio method in each season in Table 2.

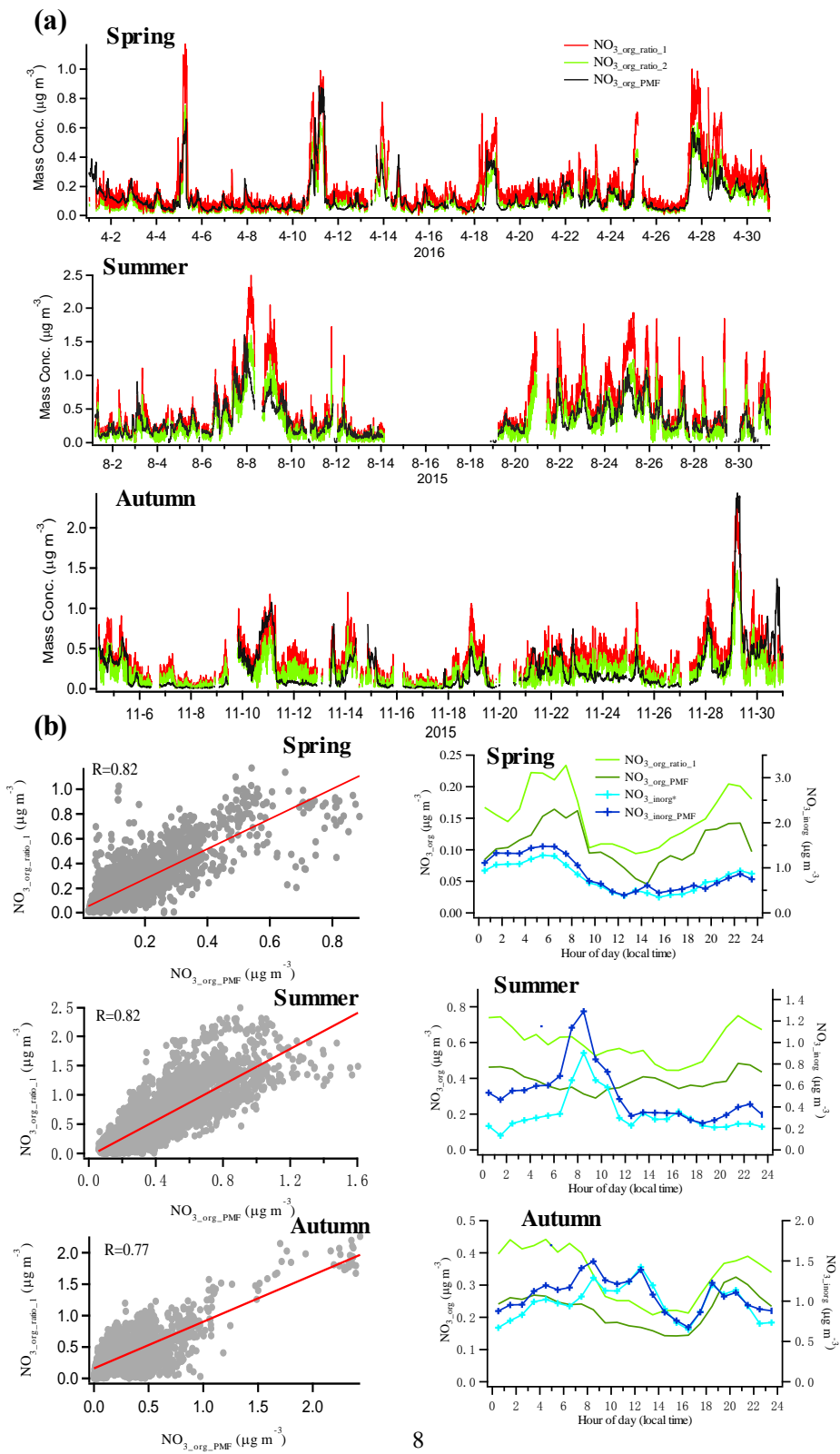
168 **Table 2.** Summary of organic nitrate estimations using the  $\text{NO}^+/\text{NO}_2^+$  ratio method and the PMF method

Sampling period	NO <sup>+</sup> /NO <sub>2</sub> <sup>+</sup> ratio method				PMF method	
	NO <sub>3,org</sub> (μg m <sup>-3</sup> ) <sup>a</sup>		NO <sub>3,org</sub> /NO <sub>3</sub>		NO <sub>3,org</sub> (μg m <sup>-3</sup> ) <sup>b</sup>	NO <sub>3,org</sub> /NO <sub>3</sub>
	lower	upper	lower	upper		
<b>Spring</b>	0.12	0.19	13%	21%	0.12	12%
<b>Summer</b>	0.34	0.53	41%	64%	0.39	43%
<b>Autumn</b>	0.21	0.33	16%	25%	0.21	16%
<b>Winter</b>	/	/	/	/	0.07	4.2%

169 <sup>a</sup> NO<sub>3,org</sub> for upper bound is denoted as NO<sub>3,org\_ratio\_1</sub>, and NO<sub>3,org</sub> for lower bound is denoted as NO<sub>3,org\_ratio\_2</sub>.

170 <sup>b</sup> NO<sub>3,org</sub> estimated using the PMF method is denoted as NO<sub>3,org\_PMF</sub>.

171 To further verify the reliability of the estimated results of organic nitrates, the NO<sub>3,org</sub> concentration time series calculated by  
 172 the two methods in each season are shown in Figure 2a, and their correlation coefficient (R) is good (0.82 for spring, 0.82 for  
 173 summer and 0.77 for autumn), indicating that similar results were achieved. The inorganic nitrate (NO<sub>3,inorg</sub><sup>\*</sup>) obtained by  
 174 subtracting NO<sub>3,org\_ratio\_1</sub> from total measured nitrates also correlated well with the inorganic nitrate estimated using the PMF  
 175 method (R=0.92 for spring, 0.87 for summer and 0.86 for autumn). Furthermore, the diurnal trends of organic nitrates obtained  
 176 by the two methods were also similar in each season, generally with lower concentrations in the daytime and higher  
 177 concentrations at night, while they were distinctive from those of inorganic nitrate (Figure 2b), supporting that organic nitrates  
 178 had been well separated from inorganic nitrate in this study.

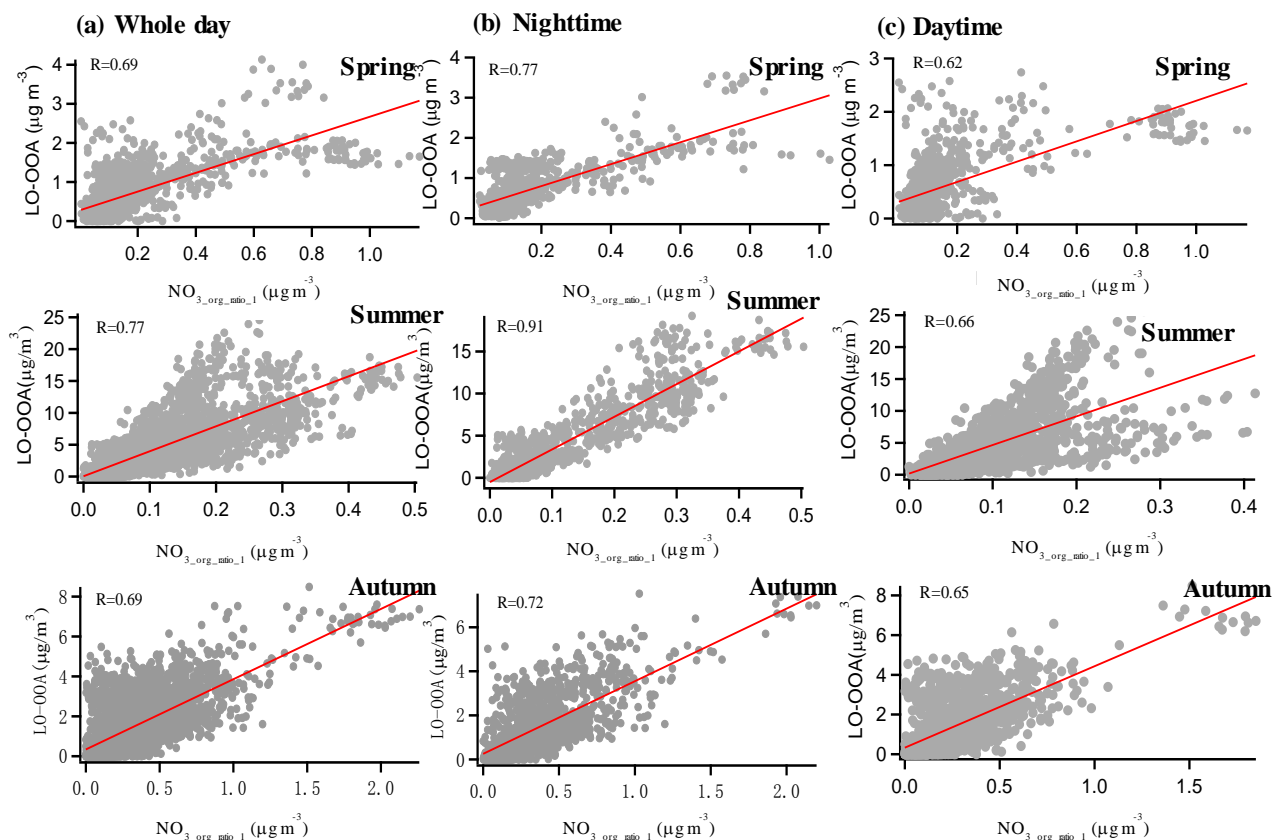




180 **Figure 2.** (a) Time series of  $\text{NO}_{3,\text{org}}$  concentration estimated by the  $\text{NO}^+/\text{NO}_2^+$  ratio method and PMF method for each  
 181 season; (b) correlations between  $\text{NO}_{3,\text{org\_ratio\_1}}$  and  $\text{NO}_{3,\text{org\_PMF}}$  (left panel); diurnal trends of organic nitrates and  $\text{NO}_{3,\text{org}}$   
 182 estimated by the different methods (right panel).

### 183 3.2 Correlation between organic nitrates and OA factors

184 As indicated by the results in the PMF method, the majority of organic nitrates were associated with LO-OOA in spring,  
 185 summer and autumn in the urban atmosphere in Shenzhen, implying a dominant secondary origin of organic nitrates. To further  
 186 confirm this relationship, we made the correlation analysis between organic nitrates estimated by the  $\text{NO}^+/\text{NO}_2^+$  ratio method  
 187 and the three factors resolved by the PMF analysis with only organic mass spectra in the three seasons. Generally, organic  
 188 nitrates were indeed found better-correlated with LO-OOA ( $R=0.69-0.77$  in Figure 3) than with HOA and MO-OOA ( $R=0.03-$   
 189  $0.69$  in Figures S6-S8), consistent with the fact that the majority of organic nitrates were associated with LO-OOA in the PMF  
 190 method. However, the moderate correlation between organic nitrates and HOA implied possibility of direct emissions of  
 191 organic nitrates. Furthermore, we found a noticeably improved correlation between LO-OOA and organic nitrates at night  
 192 (19:00-6:00) and a reduced correlation during the daytime (7:00-18:00) in Figure 3, especially in summer, implying that  
 193 organic nitrates formation might be more closely related to secondary formation at night.

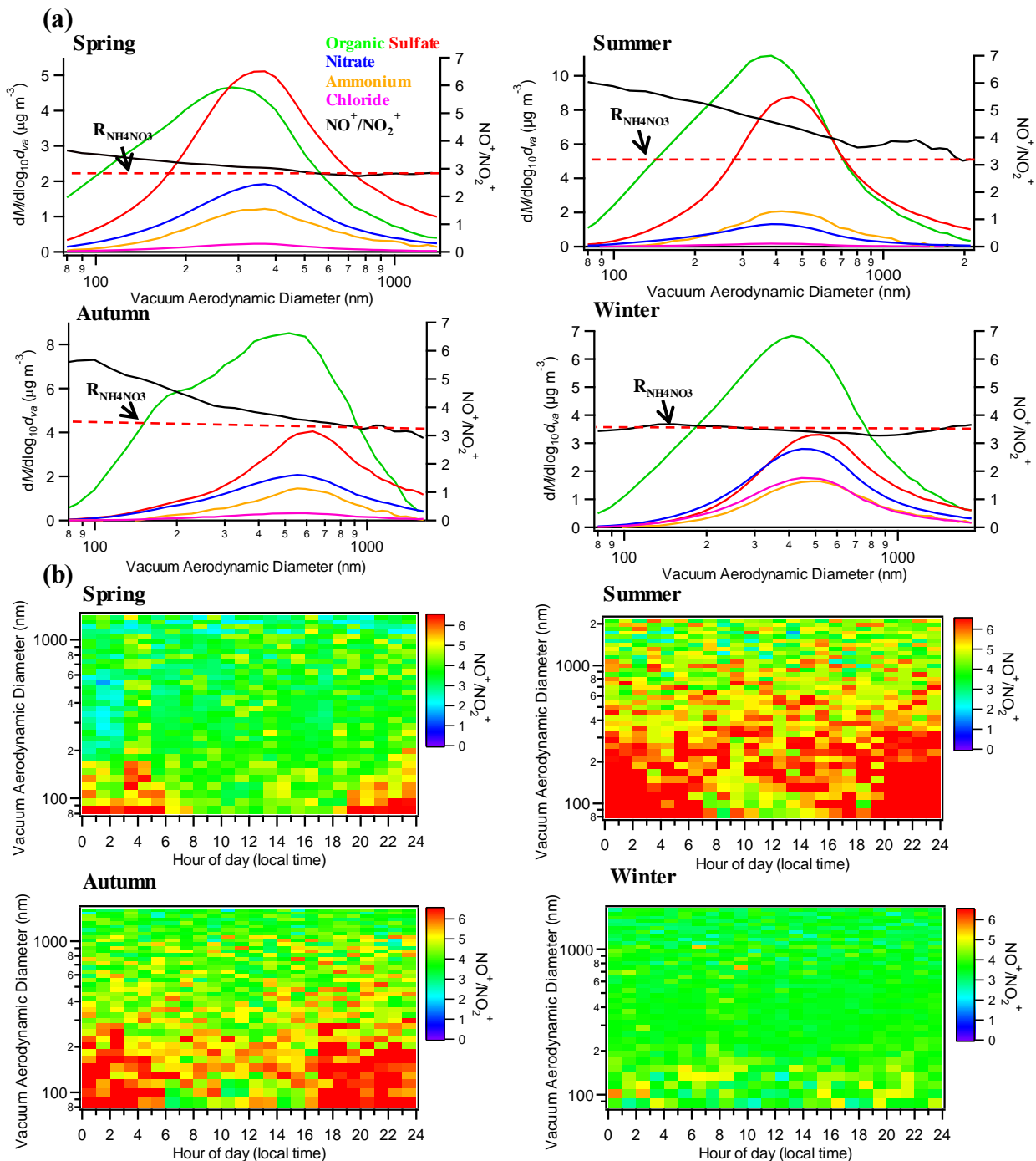


194

195 **Figure 3.**Correlation of  $\text{NO}_3\text{-org\_ratio}_1$  and LO-OOA in each season for the whole day (a), at night (b) and in the daytime (c).

### 196 **3.3 Size distribution characteristics of organic nitrates**

197 In this section, we used the  $\text{NO}^+/\text{NO}_2^+$  ratio as an indicator to investigate the size distribution characteristics of organic nitrates.  
198 The average size distributions of different aerosol species and  $\text{NO}^+/\text{NO}_2^+$  ratio in four seasons are shown in Figure 4. It is  
199 clearly found that the  $\text{NO}^+/\text{NO}_2^+$  ratio generally increased towards smaller size in spring, summer and autumn, while the  
200  $\text{NO}^+/\text{NO}_2^+$  ratio kept similar to the value of  $R_{\text{NH}_4\text{NO}_3}$  throughout the full size range in winter. It should also be noted that in  
201 spring, summer and autumn, the lowest values of  $\text{NO}^+/\text{NO}_2^+$  ratio occurring at  $>1 \mu\text{m}$  were approximate to the corresponding  
202 seasonal values of  $R_{\text{NH}_4\text{NO}_3}$ . These characteristics clearly indicated that organic nitrates occurred mostly in fresh particles with  
203 smaller sizes and thus should be mainly of local origin. Different from the bulk OA and inorganic species, organic nitrates  
204 seemed to exist scarcely in larger aged particles, implying that they could be easily removed by deposition and/or chemical  
205 degradation during air mass transport. In addition, the diurnal trends of size distribution of  $\text{NO}^+/\text{NO}_2^+$  ratio in spring, summer  
206 and autumn in Figure 4 show apparent higher values at small sizes at night, suggesting an important nighttime local origin of  
207 organic nitrates. Combining with the analysis in section 3.2, local nighttime secondary formation of organic nitrates in warmer  
208 seasons in the urban polluted atmosphere in Shenzhen is highlighted. This is well consistent with the previous findings in the  
209 US and Europe that the nighttime  $\text{NO}_3+\text{VOCs}$  reactions serve as an important source for particulate organic nitrates (Rollins  
210 et al., 2012; Xu et al., 2015a, 2015b; Fry et al., 2013; Lee et al., 2016). We will then explore the nighttime  $\text{NO}_3+\text{VOCs}$  reactions  
211 in Shenzhen in the following section.



212 **Figure 4.**(a) Average size distributions of aerosol species and  $\text{NO}^+/\text{NO}_2^+$  ratio (red dotted line represents  $R_{\text{NH}_4\text{NO}_3}$ ); (b) diurnal  
 213 trends of size distribution of  $\text{NO}^+/\text{NO}_2^+$  ratio.  
 214

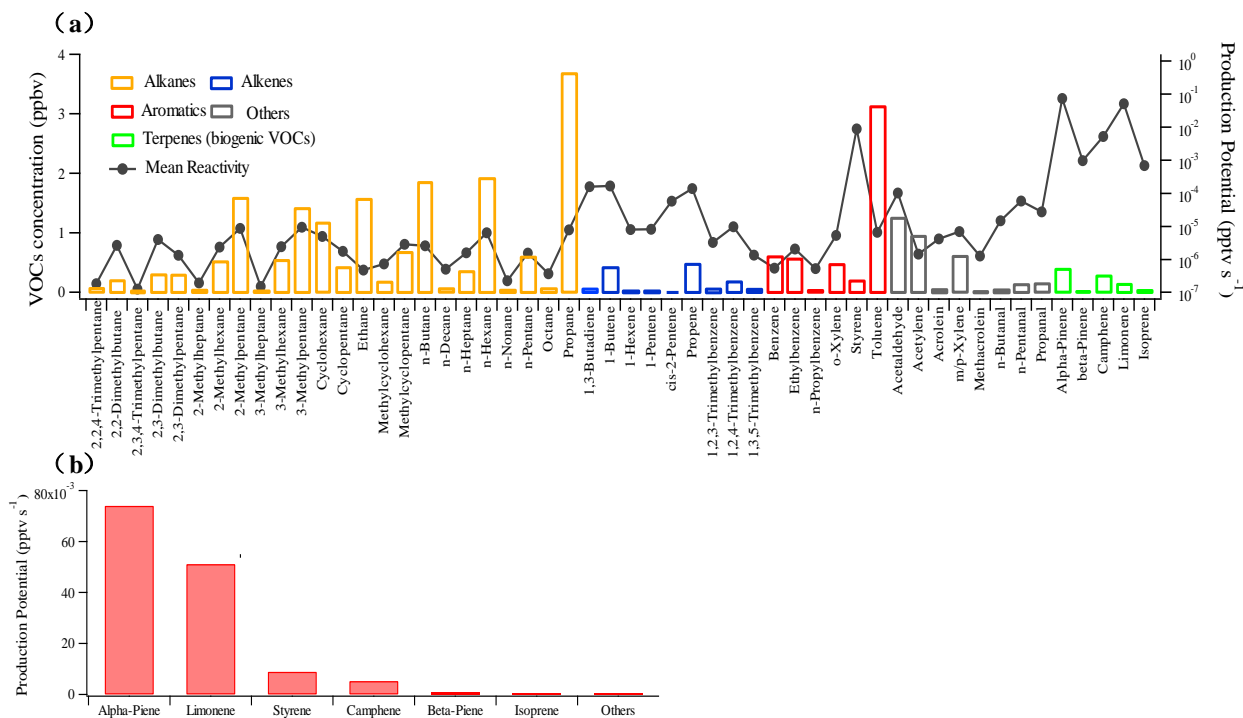
### 215 3.4 Nighttime particulate organic nitrate formation via NO<sub>3</sub>+VOCs

216 Since on-line VOCs measurement was only performed during the spring campaign, as described in section 2.2, the following  
217 theoretical analysis of NO<sub>3</sub>+VOCs reactions will be just applied to the spring case. NO<sub>3</sub>+VOCs reactions would yield a large  
218 mass of gas- and particle-phase organic nitrates (Rollins et al., 2012; Nah et al., 2016; Boyd et al., 2015, 2017; Xu et al., 2015a,  
219 2015b; Lee et al., 2016). We used the NO<sub>3</sub> loss rate at night, which can be calculated as  $K_i \cdot [VOC_i]$  in Eq. (9), to roughly judge  
220 the production potential of organic nitrates from a NO<sub>3</sub>+VOC reaction:

$$221 \quad [\text{Production Potential}]_{\text{NO}_3+\text{VOC}_i} = K_i \cdot [VOC_i] \cdot [NO_3] \quad (9)$$

222 Where  $K_i$  represents the reaction rate coefficient for NO<sub>3</sub> radical and a VOC,  $[VOC_i]$  is the concentration of the specific VOC  
223 and  $[NO_3]$  is the concentration of NO<sub>3</sub> radical. In the spring campaign, the diurnal variations of NO<sub>2</sub>, O<sub>3</sub> and estimated NO<sub>3</sub>  
224 radical concentrations are shown in Figure S10. It was found that the high concentrations of NO<sub>2</sub> ( $19.93 \pm 2.31$  ppb) at night  
225 led to high yield of NO<sub>3</sub> radical ( $1.24 \pm 0.76$  ppt) in Shenzhen, as calculated in Text S1, compared to nighttime NO<sub>3</sub> radical  
226 concentrations reported in literature in the United States (Rollins et al., 2012; Xu et al., 2015a).

227 Typical measured nighttime VOC concentrations, their reaction rate coefficients with NO<sub>3</sub> radical and the production potentials  
228 calculated are listed in Table S3 and shown in Figure 5. These VOCs were considered based on their higher ambient  
229 concentrations and availability for reaction kinetics with NO<sub>3</sub> radical. According to the distribution of production potential,  
230 five biogenic VOCs (BVOCs) (i.e.,  $\alpha$ -pinene, limonene, camphene,  $\beta$ -pinene and isoprene) and one anthropogenic VOC  
231 (styrene) were identified as notable VOC precursors with high production potential, while the sum of production potential  
232 from the other VOCs was negligible as shown in Figure 5b.



233

234

**Figure 5.** (a) Mean concentrations of VOCs and the corresponding calculated production potential of  $\text{NO}_3+\text{VOC}$  at night during the spring campaign; (b) production potential ranking of VOCs at night during the spring campaign.

235

236

Figure 6 shows the average nighttime variations of BC, LO-OOA,  $\text{NO}_{3,\text{org\_ratio}_1}$ ,  $\text{NO}_{3,\text{org\_PMF}}$  and production potential of the six notable VOCs identified during the spring campaign. The concentrations of BC and LO-OOA generally decreased slowly after sunset till sunrise due to the combined effect of both the planetary boundary layer variation and traffic emissions, while particulate organic nitrates showed a different trend with two clear growth processes (19:00-22:00 and 3:00-6:00) at night, suggesting their unique sources. In contrast, the production potentials of the six notable VOCs with  $\text{NO}_3$  had two roughly similar increases at the same periods as those of particulate organic nitrates, which supported the key role of  $\text{NO}_3+\text{VOCs}$  reactions for nighttime organic nitrate formation.

237

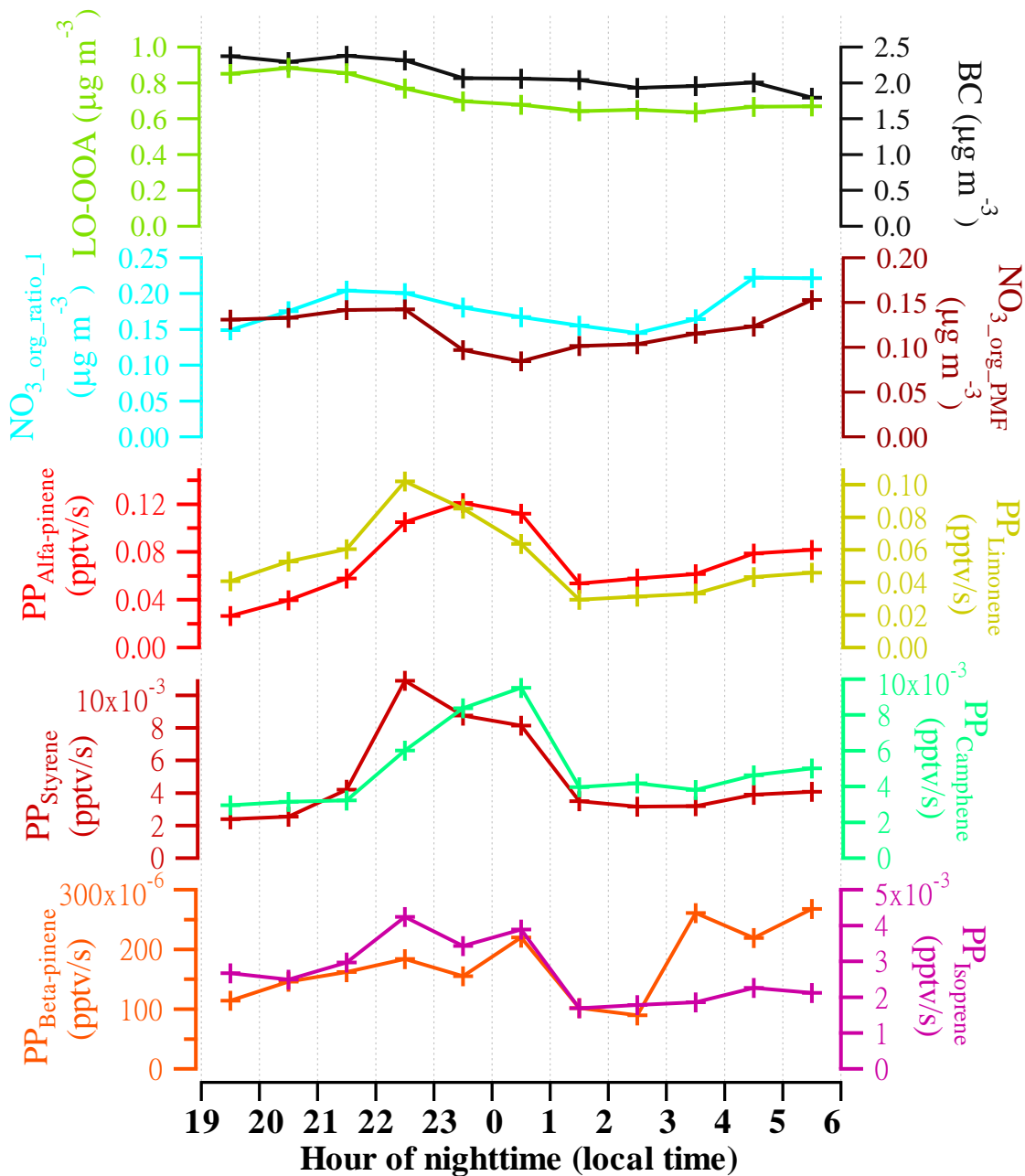
238

239

240

241

242



243

244

**Figure 6.** Nighttime variations of BC, LO-OOA, NO<sub>3.org\_ratio\_1</sub>, NO<sub>3.org\_PMF</sub> and production potential (PP) of six notable VOCs during the spring campaign.

245

246

Based on the production potential evaluation above, we further explore SOA yield of NO<sub>3</sub>+the six notable VOC precursors according to the analysis method of particulate organic nitrate formation in Xu et al. (2015a). Briefly, NO<sub>3</sub> and ozone are two main oxidants for SOA formation from VOCs at night. Based on the concentrations of oxidants and the reaction rate constants

247

248

249 for VOCs with NO<sub>3</sub> and ozone, the branching ratio of each VOC that reacts with NO<sub>3</sub> can be estimated as in Eq. (10). By  
 250 combining the estimated branching ratios and SOA yields from chamber studies (Table 3), SOA from these VOCs can be  
 251 calculated as in Eq. (11) (Xu et al., 2015a):

$$252 \quad \text{branching ratio}_{\text{species } i + \text{NO}_3} = \frac{k_{[\text{species } i + \text{NO}_3] \times [\text{NO}_3]}}{k_{[\text{species } i + \text{NO}_3] \times [\text{NO}_3]} + k_{[\text{species } i + \text{O}_3] \times [\text{O}_3]}} \quad (10)$$

$$253 \quad [\text{SOA}]_{\text{species, oxidant}} = [\text{species}] \times \text{branching ratio}_{\text{species, oxidant}} \times \text{yield}_{\text{species, oxidant}} \quad (11)$$

254 The results in Table 3 show that all the six notable VOC species were prone to react with NO<sub>3</sub> radical instead of O<sub>3</sub> at night,  
 255 and the estimated SOA production from NO<sub>3</sub>+VOCs reactions using SOA mass yields in the literature was 0-0.33 μg m<sup>-3</sup> for  
 256 α-pinene, 0.09-1.28 μg m<sup>-3</sup> for limonene, 0.24 μg m<sup>-3</sup> for styrene, 0.004-0.06 μg m<sup>-3</sup> for β-pinene and 0.002-0.02 μg m<sup>-3</sup> for  
 257 isoprene. The SOA yield from camphene is currently unknown in the literature. It is seen that the average observed nighttime  
 258 concentration of particulate organic nitrates during the spring campaign (0.39-0.83 μg m<sup>-3</sup>, converting NO<sub>3,org\_ratio\_1</sub>, NO<sub>3,org\_PMF</sub>  
 259 in Figure 6 into organic nitrates assuming the average molecular weight of organic nitrates of 200 to 300 g mol<sup>-1</sup>) was well  
 260 within the estimated SOA concentration ranges produced by α-pinene, limonene and styrene in Table 3, indicating that these  
 261 three VOCs were the key VOC precursors in urban atmosphere in Shenzhen. Considering both the production potentials and  
 262 SOA yields, the contributions of β-pinene and isoprene to nighttime formation of particulate organic nitrates could be  
 263 negligible.

264 **Table 3.** Average concentrations, reaction branching and SOA production of α-pinene, limonene, styrene, camphene, β-  
 265 pinene and isoprene with respect to different oxidants at night in the spring campaign.

Species	Concentration (ppbv)	Rate coefficient <sup>a</sup>		Branching ratio		SOA yield from the literature (with NO <sub>3</sub> )	SOA from VOCs + NO <sub>3</sub> (μg m <sup>-3</sup> )
		NO <sub>3</sub>	O <sub>3</sub>	NO <sub>3</sub>	O <sub>3</sub>		
<b>α-pinene</b>	0.39	6.64E-12	7.2E-17	0.962	0.038	0-0.16 <sup>b</sup>	0-0.33
<b>Limonene</b>	0.14	1.22E-11	1.54E-16	0.957	0.043	0.12-1.74 <sup>c</sup>	0.09-1.28
<b>Styrene</b>	0.19	1.50E-12	1.70E-17	0.941	0.059	0.23 <sup>d</sup>	0.24
<b>Camphene</b>	0.28	6.20E-13	9.0E-19	0.992	0.008	/	/
<b>β-pinene</b>	0.01	2.51E-12	1.50E-17	0.968	0.032	0.07-1.04 <sup>e</sup>	0.004-0.06
<b>Isoprene</b>	0.032	6.96E-13	1.27E-17	0.908	0.091	0.02-0.24 <sup>f</sup>	0.002-0.02

266 <sup>a</sup> Rate coefficients for all species except camphene are from the Master Chemical Mechanism model  
 267 (<http://mcm.leeds.ac.uk/MCM/>; under 25 °C), rate coefficients for camphene are from Martínez et al. (1999) and Atkinson et  
 268 al. (1990).

269 <sup>b</sup> Hallquist et al. (1999); Spittler et al. (2006); Perraud et al. (2010); Fry et al. (2014); Nah et al. (2016).

270 <sup>c</sup> Fry et al. (2011, 2014); Spittler et al. (2006); Boyd et al. (2017).

271 <sup>d</sup> Cabrera-Perez et al. (2017).

272 <sup>e</sup> Griffin et al. (1999); Fry et al. (2009); Fry et al. (2014); Boyd et al. (2015).

273 <sup>f</sup> Rollins et al. (2009); Ng et al. (2008).

274 It should be noted that, all previous studies on nighttime organic nitrate formation in the US and Europe focused on mechanisms  
275 of NO<sub>3</sub> reactions with BVOCs (Hallquist et al., 1999; Spittler et al., 2006; Perraud et al., 2010; Fry et al., 2014; Nah et al., 2016;  
276 Boyd et al., 2015, 2017). In this study, however, we found that styrene, one of major aromatics derived from anthropogenic  
277 emissions (Cabrera-Perez et al., 2016), served as a key VOC precursor for organic nitrate formation in Shenzhen, theoretically  
278 with comparable SOA producing ability to those of  $\alpha$ -pinene and limonene and much higher ability than those of  $\beta$ -pinene and  
279 isoprene. In China, styrene has been actually identified as an important VOC of non-methane hydrocarbons (NMHCs) in urban  
280 areas, and has a notable contribution to ozone formation and SOA production (An et al., 2009; Yuan et al., 2013; Zhu et al.,  
281 2019). This study further highlights the key role of this anthropogenic VOC precursor in nighttime particulate organic nitrate  
282 formation in urban atmosphere in China, and relevant smog chamber studies for anthropogenic VOCs+NO<sub>3</sub> reactions are  
283 needed to support parameterization in modeling.

### 284 **3.5 Comparison with other similar studies and implications**

285 Table 4 shows the average ambient temperatures, average concentrations of NO, NO<sub>2</sub>, monoterpenes, NO<sub>3,org</sub>, the ratio of  
286 NO<sub>3,org</sub> to NO<sub>3,total</sub> and the ratio of organic nitrates to total organics in a few similar field campaigns available in the literature,  
287 which all found the key role of NO<sub>3</sub>+VOCs reactions for nighttime particulate organic nitrate formation. Generally, the  
288 concentrations of particulate organic nitrates varied less than an order of magnitude (0.06-0.98  $\mu\text{g}/\text{m}^3$ ) among the different  
289 sites. Higher concentrations of particulate organic nitrates generally corresponded to higher NO<sub>x</sub> concentrations rather than  
290 BVOC concentrations, implying that the formation of particulate organic nitrates is more likely NO<sub>x</sub>-limited than BVOCs-  
291 limited. Note that, particulate organic nitrates constituted the major part (86-100%) of total nitrates in the atmosphere scarce  
292 of NO<sub>x</sub> (in Centreville and Woodland Park), suggesting that NO<sub>x</sub> was very quickly consumed to form particulate organic  
293 nitrates and thus the formation of particulate organic nitrates should be NO<sub>x</sub>-limited. On the other hand, although the BVOC  
294 concentrations in Bakersfield were far less than in the other campaigns, the concentration of particulate organic nitrates there  
295 showed a medial level among all the campaigns. In the spring campaign of this study, we examined the correlation between  
296 organic nitrates and NO<sub>2</sub> or VOCs (by the sum of  $\alpha$ -pinene, limonene and styrene) at night (Figure S11) and found a significant  
297 correlation of organic nitrates with NO<sub>2</sub> (R=0.40-0.47) rather than with VOCs (R=0.06-0.20), implying a dominant role of  
298 NO<sub>x</sub> in the organic nitrate formation. Therefore, it is inferred that formation of particulate organic nitrates through BVOC  
299 reactions may be indirectly NO<sub>x</sub>-controlled, and high NO<sub>x</sub> emissions could promote biogenic SOA formation at night.



300 **Table 4.** Average ambient temperatures, average concentrations of monoterpenes,  $\text{NO}_{3,\text{total}}$ ,  $\text{NO}_{3,\text{org}}$ ,  $\text{NO}_{3,\text{org}}/\text{NO}_{3,\text{total}}$  and the ratio of organic nitrates to total organics (ON/Org) for different  
 301 field campaigns around the world. The ON results at the European and US sites are from Kiendler-Scharr et al. (2016) and Ng et al. (2017).

Sampling site	Site type	Sampling period	Temperature (°C)	NO (ppbv)	NO <sub>2</sub> (ppbv)	Monoterpenes (ppbv)	NO <sub>3,org</sub> (µg m <sup>-3</sup> )	NO <sub>3,org</sub> /NO <sub>3,total</sub>	ON/Org	Reference/Note
Bakersfield, US	rural	May-June, 2010	23.0		8.2	0.045 ( $\alpha$ -pinene) 0.004 ( $\beta$ -pinene) 0.034 (limonene)	0.16	0.28	0.23	Rollins et al. (2012)/ NO <sub>3,org</sub> measured by TD-LIF
Woodland Park, US	high attitude	July-August, 2011	15.0		1.2	0.25 (monoterpene)	0.06	0.86	0.09	Fry et al. (2013)/ Use AMS data to estimate NO <sub>3,org</sub>
Centreville, US	rural	June-July, 2013	24.7	0.1	1.1	0.350 ( $\alpha$ -pinene)* 0.312 ( $\beta$ -pinene)* 0.050 (limonene)*	0.08	1.00	0.10	Xu et al. (2015a)  Xu et al. (2015b)/ Use AMS data to estimate NO <sub>3,org</sub>
Barcelona, Spain	urban	March, 2009	13.3	11.0	23.6	0.423 (monoterpene)	0.48	0.13	0.13	Mohr et al. (2012)  Pandolfi et al. (2014) / Use AMS data to estimate NO <sub>3,org</sub>
Shenzhen, China	urban	April, 2016	24.5	8.0	19.4	0.391 ( $\alpha$ -pinene)* 0.013 ( $\beta$ -pinene)* 0.137 (limonene)*	0.16	0.17	0.11	This study/ Use AMS data to estimate NO <sub>3,org</sub>

302 \*BVOC concentration at night.

#### 303 4. Conclusions

304 An Aerodyne HR-ToF-AMS was deployed in urban Shenzhen for about one month per season during 2015–2016 to  
305 characterize particulate organic nitrates with high time resolution. We found that the mass fractions of organic nitrates in total  
306 organics were substantial during warmer seasons, including spring (9-21%), summer (11-25%) and autumn (9-20%), while  
307 particulate organic nitrates were negligible in winter. The correlation analysis between organic nitrates and each OA factor  
308 showed higher correlation ( $R=0.77$  in spring,  $0.91$  in summer and  $0.72$  in autumn) between organic nitrates and LO-OOA at  
309 night. The diurnal trend analysis of size distribution of  $\text{NO}^+/\text{NO}_2^+$  ratio further suggested that organic nitrate formation mainly  
310 occurred at night, and also presented that organic nitrates concentrated on smaller sizes, suggesting that they were mostly local  
311 product. The calculated theoretical nighttime production potential of  $\text{NO}_3$  reactions with VOCs measured in spring showed  
312 that six VOC species (i.e.,  $\alpha$ -pinene, limonene, styrene, camphene,  $\beta$ -pinene and isoprene) were notable precursors. The SOA  
313 yield analysis further indicated that  $\alpha$ -pinene, limonene and styrene contributed mostly to nighttime formation of particulate  
314 organic nitrates in spring in Shenzhen, highlighting the unique contribution of anthropogenic VOCs in comparison with  
315 previous studies in the US and Europe. Finally, the comparison of the results in this study with other similar studies implied  
316 that nighttime formation of particulate organic nitrates is more likely  $\text{NO}_x$ -limited than VOCs-limited.

#### 317 Acknowledgments

318 This work was supported by National Key R&D Program of China (2018YFC0213901), National Natural Science Foundation  
319 of China (91544215; 41622304) and Science and Technology Plan of Shenzhen Municipality (JCYJ20170412150626172).

#### 320 References

- 321 An, J. L., Wang, Y. S., Sun, Y.: Effects of nonmethane hydrocarbons on ozone formation in Beijing. *Ecology & Environmental*  
322 *Sciences*.
- 323 Atkinson, R., Aschmann, S. M., Arey, J.: Rate constants for the gas-phase reactions of OH and  $\text{NO}_3$  radicals and  $\text{O}_3$  with  
324 sabinene and camphene at  $296\pm 2$  K. *Atmospheric Environment. Part A. General Topics*, 24, (10), 2647-2654,  
325 [https://doi.org/10.1016/0960-1686\(90\)90144-C](https://doi.org/10.1016/0960-1686(90)90144-C), 1990
- 326 Ayres, B.R., Allen, H.M., Draper, D.C., Brown, S.S., Wild, R.J., Jimenez, J.L., Day, D.A., Campuzano-Jost, P., Hu, W., De  
327 Gouw, J.A., Koss, A., Cohen, R.C., Duffey, K.C., Romer, P., Baumann, K., Edgerton, E., Takahama, S., Thornton, J.A.,  
328 Lee, B.H., Lopez-Hilfiker, F.D., Mohr, C., Wennberg, P.O., Nguyen, T.B., Teng, A.P., Goldstein, A.H., Olson, K., Fry,  
329 J.L.: Organic nitrate aerosol formation via  $\text{NO}_3^+$  biogenic volatile organic compounds in the southeastern United States.  
330 *Atmos. Chem. Phys.* 15, 13377-13392. <https://doi.org/10.5194/acp-15-13377-2015>, 2015.

331 Boyd, C.M., Nah, T., Xu, L., Berkemeier, T., Ng, N.L.: Secondary Organic Aerosol(SOA) from Nitrate Radical Oxidation of  
332 Monoterpenes: Effects of Temperature, Dilution, and Humidity on Aerosol Formation, Mixing, and Evaporation. *Environ.*  
333 *Sci. Technol.* 51, 7831–7841. <https://doi.org/10.1021/acs.est.7b01460>, 2017.

334 Boyd, C.M., Sanchez, J., Xu, L., Eugene, A.J., Nah, T., Tuet, W.Y., Guzman, M.I., Ng, N.L.: Secondary organic aerosol  
335 formation from the  $\beta$ -pinene+NO<sub>3</sub> system: effect of humidity and peroxy radical fate. *Atmos. Chem. Phys.* 15, 7497-  
336 7522. <https://doi.org/10.5194/acp-15-7497-2015>, 2015.

337 Bruns, E.A., Perraud, V., Zelenyuk, A., Ezell, M.J., Johnson, S.N., Yu, Y., Imre, D., Finlayson-Pitts, B.J., Alexander, M.L.:  
338 Comparison of FTIR and particle mass spectrometry for the measurement of particulate organic nitrates. *Environ. Sci.*  
339 *Technol.* 44, 1056-1061. <https://doi.org/10.1021/es9029864>, 2010.

340 Cabrera-Perez, D., Taraborrelli, D., Sander, R., and Pozzer, A.: Global atmospheric budget of simple monocyclic aromatic  
341 compounds, *Atmos. Chem. Phys.*, 16, 6931-6947, <https://doi.org/10.5194/acp-16-6931-2016>, 2016.

342 Cabrera-Perez, D., Taraborrelli, D., Lelieveld, J., Hoffmann, T., and Pozzer, A.: Global impact of monocyclic aromatics on  
343 tropospheric composition, *Atmos. Chem. Phys. Discuss.*, <https://doi.org/10.5194/acp-2017-928>, 2017.

344 Canagaratna, M.R., Jayne, J.T., Jimenez, J.L., Allan, J.D., Alfarra, M.R., Zhang, Q., Onasch, T.B., Drewnick, F., Coe, H.,  
345 Middlebrook, A., Delia, A., Williams, L.R., Trimborn, A.M., Northway, M.J., DeCarlo, P.F., Kolb, C.E., Davidovits, P.,  
346 Worsnop, D.R.: Chemical and microphysical characterization of ambient aerosols with the aerodyne aerosol mass  
347 spectrometer. *Mass Spectrom. Rev.* 26, 185-222. <https://doi.org/10.1002/mas.20115>, 2007.

348 Cubison, M. J., Ortega, A. M., Hayes, P. L., Farmer, D. K., Day, D., Lechner, M. J., Brune, W. H., Apel, E., Diskin, G. S.,  
349 Fisher, J. A., Fuelberg, H. E., Hecobian, A., Knapp, D. J., Mikoviny, T., Riemer, D., Sachse, G. W., Sessions, W., Weber,  
350 R. J., Weinheimer, A. J., Wisthaler, A., and Jimenez, J. L.: Effects of aging on organic aerosol from open biomass burning  
351 smoke in aircraft and laboratory studies, *Atmos. Chem. Phys.*, 11, 12049-12064, [https://doi.org/10.5194/acp-11-12049-](https://doi.org/10.5194/acp-11-12049-2011)  
352 [2011](https://doi.org/10.5194/acp-11-12049-2011), 2011.

353 Day, D. A., Liu, S., Russell, L. M., and Ziemann, P. J.: Organonitrate group concentrations in submicron particles with high  
354 nitrate and organic fractions in coastal southern California, *Atmos. Environ.*, 44, 1970–1979,  
355 <https://doi.org/10.1016/j.atmosenv.2010.02.045>, 2010.

356 DeCarlo, P.F., Kimmel, J.R., Trimborn, A., Northway, M.J., Jayne, J.T., Aiken, A.C., Gonin, M., Fuhrer, K., Horvath, T.,  
357 Docherty, K.S., Worsnop, D.R., Jimenez, J.L.: Field-deployable, high-resolution, time-of-flight aerosol mass  
358 spectrometer. *Anal. Chem.* 78, 8281-8289. <https://doi.org/10.1021/ac061249n>, 2006.

359 Farmer, D.K., Matsunaga, A., Docherty, K.S., Surratt, J.D., Seinfeld, J.H., Ziemann, P.J., Jimenez, J.L.: Response of an aerosol  
360 mass spectrometer to organonitrates and organosulfates and implications for atmospheric chemistry. *Proc. Natl. Acad.*  
361 *Sci.* 107, 6670-6675. <https://doi.org/10.1073/pnas.0912340107>, 2010.

362 Fry, J.L., Draper, D.C., Barsanti, K.C., Smith, J.N., Ortega, J., Winkler, P.M., Lawler, M.J., Brown, S.S., Edwards, P.M.,  
363 Cohen, R.C.: Secondary Organic Aerosol Formation and Organic Nitrate Yield from NO<sub>3</sub> Oxidation of Biogenic  
364 Hydrocarbons. *Environ. Sci. Technol.* 48, 11944–11953. <https://doi.org/10.1021/es502204x>, 2014.

365 Fry, J.L., Draper, D.C., Zarzana, K.J., Campuzano-Jost, P., Day, D.A., Jimenez, J.L., Brown, S.S., Cohen, R.C., Kaser, L.,  
366 Hansel, A., Cappellin, L., Karl, T., Hodzic Roux, A., Turnipseed, A., Cantrell, C., Lefer, B.L., Grossberg, N.:  
367 Observations of gas- and aerosol-phase organic nitrates at BEACHON-RoMBAS 2011. *Atmos. Chem. Phys.* 13, 8585-  
368 8605. <https://doi.org/10.5194/acp-13-8585-2013>, 2013.

369 Fry, J.L., Kiendler-Scharr, A., Rollins, A.W., Brauers, T., Brown, S.S., Dorn, H.P., Dubé, W.P., Fuchs, H., Mensah, A., Rohrer,  
370 F., Tillmann, R., Wahner, A., Wooldridge, P.J., Cohen, R. C.: SOA from limonene: Role of NO<sub>3</sub> in its generation and  
371 degradation. *Atmos. Chem. Phys.* 11, 3879-3894. <https://doi.org/10.5194/acp-11-3879-2011>, 2011.

372 Fry, J.L., Kiendlerscharr, A., Rollins, A.W., Wooldridge, P.J., Brown, S.S., Fuchs, H., Dube, W.P., Mensah, A., Dal Maso,  
373 M., Tillmann, R.: Organic nitrate and secondary organic aerosol yield from NO<sub>3</sub> oxidation of  $\beta$ -pinene evaluated using  
374 a gas-phase kinetics/aerosol partitioning model. *Atmos. Chem. Phys.* 9, 1431–1449. [https://doi.org/10.5194/acp-9-1431-](https://doi.org/10.5194/acp-9-1431-2009)  
375 [2009](https://doi.org/10.5194/acp-9-1431-2009), 2009.

376 Griffin, R. J., Cocker, D. R., III, Flagan, R. C., and Seinfeld, J. H.: Organic aerosol formation from the oxidation of biogenic  
377 hydrocarbons. *J. Geophys. Res.*, 104, 3555–3567, <https://doi.org/10.1029/1998jd100049>, 1999.

378 Hallquist, M., Wängberg, I., Ljungström, E., Barnes, I., Becker, K.H.: Aerosol and product yields from NO<sub>3</sub> radical-initiated  
379 oxidation of selected monoterpenes. *Environ. Sci. Technol.* 33, 553-559. <https://doi.org/10.1021/es980292s>, 1999.

380 Hao, L.Q., Kortelainen, A., Romakkaniemi, S., Portin, H., Jaatinen, A., Leskinen, A., Komppula, M., Miettinen, P., Sueper,  
381 D., Pajunoja, A., Smith, J.N., Lehtinen, K.E.J., Worsnop, D.R., Laaksonen, A., Virtanen, A.: Atmospheric submicron  
382 aerosol composition and particulate organic nitrate formation in a boreal forestland-urban mixed region. *Atmos. Chem.*  
383 *Phys.* 14, 13483-13495. <https://doi.org/10.5194/acp-14-13483-2014>, 2014.

384 He, L.Y., Huang, X.F., Xue, L., Hu, M., Lin, Y., Zheng, J., Zhang, R., Zhang, Y.H.: Submicron aerosol analysis and organic  
385 source apportionment in an urban atmosphere in Pearl River Delta of China using high-resolution aerosol mass  
386 spectrometry. *J. Geophys. Res. Atmos.* 116, D12. <https://doi.org/10.1029/2010JD014566>, 2011.

387 Huang, X.F., He, L.Y., Hu, M., Canagaratna, M.R., Sun, Y., Zhang, Q., Zhu, T., Xue, L., Zeng, L.W., Liu, X.G., Zhang, Y.H.,  
388 Jayne, J.T., Ng, N.L., Worsnop, D.R.: Highly time-resolved chemical characterization of atmospheric submicron particles  
389 during 2008 Beijing Olympic games using an aerodyne high-resolution aerosol mass spectrometer. *Atmos. Chem. Phys.*  
390 10, 8933-8945. <https://doi.org/10.5194/acp-10-8933-2010>, 2010.

391 Huang, X.F., He, L.Y., Xue, L., Sun, T.L., Zeng, L.W., Gong, Z.H., Hu, M., Zhu, T.: Highly time-resolved chemical  
392 characterization of atmospheric fine particles during 2010 Shanghai World Expo. *Atmos. Chem. Phys.* 12, 4897-4907.  
393 <https://doi.org/10.5194/acp-12-4897-2012>, 2012.

394 Huang, X.F., Xue, L., Tian, X.D., Shao, W.W., Sun, T. Le, Gong, Z.H., Ju, W.W., Jiang, B., Hu, M., He, L.Y.: Highly time-  
395 resolved carbonaceous aerosol characterization in Yangtze River Delta of China: Composition, mixing state and  
396 secondary formation. *Atmos. Environ.* 64, 200-207. <https://doi.org/10.1016/j.atmosenv.2012.09.059>, 2013.

397 Jimenez, J. L., Jayne, J. T., Shi, Q., Kolb, C. E., Worsnop, D. R., Yourshaw, I., Seinfeld, J. H., Flagan, R. C., Zhang, X. F.,  
398 Smith, K. A., Morris, J. W., and Davidovits, P.: Ambient aerosol sampling using the aerodyne aerosol mass spectrometer,  
399 *J. Geophys. Res.-Atmos.*, 108, 447–457, <https://doi.org/10.1029/2001JD001213>, 2003.

400 Kiendler-Scharr, A., Mensah, A. A., Friese, E., Topping, D., Nemitz, E., Prevot, A. S. H., Äijälä, M., Allan, J., Canonaco, F.,  
401 Canagaratna, M., Carbone, S., Crippa, M., Dall'Osto, M., Day, D. A., De Carlo, P., Di Marco, C. F., Elbern, H., Eriksson,  
402 A., Freney, E., Hao, L., Herrmann, H., Hildebrandt, L., Hillamo, R., Jimenez, J. L., Laaksonen, A., McFiggans, G., Mohr,  
403 C., O'Dowd, C., Otjes, R., Ovadnevaite, J., Pandis, S. N., Poulain, L., Schlag, P., Sellegri, K., Swietlicki, E., Tiitta, P.,  
404 Vermeulen, A., Wahner, A., Worsnop, D., and Wu, H. C.: Organic nitrates from night-time chemistry are ubiquitous in  
405 the European submicron aerosol, *Geophys. Res. Lett.*, 43, 7735–7744, <https://doi.org/10.1002/2016GL069239>, 2016.

406 Lee, B.H., Mohr, C., Lopez-Hilfiker, F.D., Lutz, A., Hallquist, M., Lee, L., Romer, P., Cohen, R.C., Iyer, S., Kurten, T., Hu,  
407 W., Day, D.A., Campuzano-Jost, P., Jimenez, J.L., Xu, L., Ng, N.L., Guo, H., Weber, R.J., Wild, R.J., Brown, S.S., Koss,  
408 A., de Gouw, J., Olson, K., Goldstein, A.H., Seco, R., Kim, S., McAvey, K., Shepson, P.B., Starn, T., Baumann, K.,  
409 Edgerton, E.S., Liu, J., Shilling, J.E., Miller, D.O., Brune, W., Schobesberger, S., D'Ambro, E.L., Thornton, J.A.: Highly  
410 functionalized organic nitrates in the southeast United States: Contribution to secondary organic aerosol and reactive  
411 nitrogen budgets. *Proc. Natl. Acad. Sci.* 113, 1516-1521. <https://doi.org/10.1073/pnas.1508108113>, 2016.

412 Lelieveld, J., Gromov, S., Pozzer, A., Taraborrelli, D.: Global tropospheric hydroxyl distribution, budget and reactivity. *Atmos.*  
413 *Chem. Phys.* 16, 12477-12493. <https://doi.org/10.5194/acp-16-12477-2016>, 2016.

414 Martínez, E.; Cabañas, B.; Aranda, A.; Martín, P.; Salgado, S.: Absolute Rate Coefficients for the Gas-Phase Reactions of  
415 NO<sub>3</sub> Radical with a Series of Monoterpenes at T = 298 to 433 K. *Journal of Atmospheric Chemistry*, 33, (3), 265-282.  
416 <https://doi.org/10.1023/A:1006178530211>, 1999.

417 Middlebrook, A.M., Bahreini, R., Jimenez, J.L., Canagaratna, M.R.: Evaluation of composition-dependent collection  
418 efficiencies for the Aerodyne aerosol mass spectrometer using field data. *Aerosol Sci. Technol.* 46, 258-271.  
419 <https://doi.org/10.1080/02786826.2011.620041>, 2012.

420 Mohr, C., DeCarlo, P. F., Heringa, M. F., Chirico, R., Slowik, J. G., Richter, R., Reche, C., Alastuey, A., Querol, X., Seco, R.,  
421 Peñuelas, J., Jiménez, J. L., Crippa, M., Zimmermann, R., Baltensperger, U., and Prévôt, A. S. H.: Identification and  
422 quantification of organic aerosol from cooking and other sources in Barcelona using aerosol mass spectrometer data,  
423 *Atmos. Chem. Phys.*, 12, 1649–1665, <https://doi.org/10.5194/acp-12-1649-2012>, 2012.

424 Nah, T., McVay, R. C., Zhang, X., Boyd, C. M., Seinfeld, J. H., and Ng, N. L.: Influence of seed aerosol surface area and  
425 oxidation rate on vapor wall deposition and SOA mass yields: a case study with  $\alpha$ -pinene ozonolysis, *Atmos. Chem.*  
426 *Phys.*, 16, 9361–9379, <https://doi.org/10.5194/acp-16-9361-2016>, 2016.

427 Ng, N. L., Brown, S. S., Archibald, A. T., Atlas, E., Cohen, R. C., Crowley, J. N., Day, D. A., Donahue, N. M., Fry, J. L.,  
428 Fuchs, H., Griffin, R. J., Guzman, M. I., Herrmann, H., Hodzic, A., Iinuma, Y., Jimenez, J. L., Kiendler-Scharr, A., Lee,  
429 B. H., Luecken, D. J., Mao, J., McLaren, R., Mutzel, A., Osthoff, H. D., Ouyang, B., Picquet-Varrault, B., Platt, U., Pye,  
430 H. O. T., Rudich, Y., Schwantes, R. H., Shiraiwa, M., Stutz, J., Thornton, J. A., Tilgner, A., Williams, B. J., and Zaveri,

431 R. A.: Nitrate radicals and biogenic volatile organic compounds: oxidation, mechanisms, and organic aerosol, *Atmos.*  
432 *Chem. Phys.*, 17, 2103-2162, <https://doi.org/10.5194/acp-17-2103-2017>, 2017.

433 Ng, N. L., Canagaratna, M. R., Zhang, Q., Jimenez, J. L., Tian, J., Ulbrich, I. M., Kroll, J. H., Docherty, K.S., Chhabra, P.S.,  
434 Bahreini, R., Murphy, S.M., Seinfeld, J.H., Hildebrandt, L., Donahue, N.M., Decarlo, P.F., Lanz, V.A., Prévôt, A.S.H.,  
435 Dinar, E., Rudich, Y., Worsnop, D.R.: Organic aerosol components observed in Northern Hemispheric datasets from  
436 Aerosol Mass Spectrometry. *Atmos. Chem. Phys.* 10, 4625-4641. <https://doi.org/10.5194/acp-10-4625-2010>, 2010.

437 Ng, N. L., Kwan, A. J., Surratt, J. D., Chan, A. W. H., Chhabra, P. S., Sorooshian, A., Pye, H. O. T., Crouse, J. D., Wennberg,  
438 P. O., Flagan, R. C., and Seinfeld, J. H.: Secondary organic aerosol (SOA) formation from reaction of isoprene with  
439 nitrate radicals (NO<sub>3</sub>), *Atmos. Chem. Phys.*, 8, 4117–4140, <https://doi.org/10.5194/acp-8-4117-2008>, 2008.

440 Pandolfi, M.; Querol, X.; Alastuey, A.; Jimenez, J. L.; Jorba, O.; Day, D.; Ortega, A.; Cubison, M. J.; Comerón, A.; Sicard,  
441 M.; Mohr, C.; Prévôt, A. S. H.; Minguillón, M. C.; Pey, J.; Baldasano, J. M.; Burkhardt, J. F.; Seco, R.; Peñuelas, J.; van  
442 Drooge, B. L.; Artiñano, B.; Di Marco, C.; Nemitz, E.; Schallhart, S.; Metzger, A.; Hansel, A.; Lorente, J.; Ng, S.; Jayne,  
443 J.; Szidat, S.: Effects of sources and meteorology on particulate matter in the Western Mediterranean Basin: An overview  
444 of the DAURE campaign. *Journal of Geophysical Research: Atmospheres*, 119, (8), 4978-5010.  
445 <https://10.1002/2013JD021079>, 2014.

446 Perraud, V., Bruns, E. A., Ezell, M. J., Johnson, S. N., Greaves, J., and Finlayson-Pitts, B. J.: Identification of organic nitrates  
447 in the NO<sub>3</sub> radical initiated oxidation of  $\alpha$ -pinene by atmospheric pressure chemical ionization mass spectrometry,  
448 *Environ. Sci. Technol.*, 44, 5887–5893. <https://doi.org/10.1021/es1005658>, 2010.

449 Rollins, A.W., Browne, E.C., Min, K.-E., Pusede, S.E., Wooldridge, P.J., Gentner, D.R., Goldstein, A.H., Liu, S., Day, D.A.,  
450 Russell, L.M., Cohen, R.C.: Evidence for NO<sub>x</sub> Control over Nighttime SOA Formation. *Science*. 337, 1210-1212.  
451 <https://doi.org/10.1126/science.1221520>, 2012.

452 Rollins, A. W., Kiendler-Scharr, A., Fry, J. L., Brauers, T., Brown, S. S., Dorn, H.-P., Dubé, W. P., Fuchs, H., Mensah, A.,  
453 Mentel, T. F., Rohrer, F., Tilman, R., Wegener, R., Wooldridge, P. J., and Cohen, R. C.: Isoprene oxidation by nitrate  
454 radical: alkyl nitrate and secondary organic aerosol yields, *Atmos. Chem. Phys.*, 9, 6685–6703, [https://doi.org/10.5194/acp-](https://doi.org/10.5194/acp-9-6685-2009)  
455 [9-6685-2009](https://doi.org/10.5194/acp-9-6685-2009), 2009.

456 Sato, K., Takami, A., Iozaki, T., Hikida, T., Shimono, A., Imamura, T.: Mass spectrometric study of secondary organic aerosol  
457 formed from the photo-oxidation of aromatic hydrocarbons. *Atmos. Environ.* 44, 1080-1087.  
458 <https://doi.org/10.1016/j.atmosenv.2009.12.013>, 2010.

459 Sobanski, N., Thieser, J., Schuladen, J., Sauvage, C., Song, W., Williams, J., Lelieveld, J., Crowley, J.N.: Day and night-time  
460 formation of organic nitrates at a forested mountain site in south-west Germany. *Atmos. Chem. Phys.* 17, 4115-4130.  
461 <https://doi.org/10.5194/acp-17-4115-2017>, 2017.

462 Spittler, M., Barnes, I., Bejan, I., Brockmann, K.J., Benter, T., Wirtz, K.: Reactions of NO<sub>3</sub> radicals with limonene and  $\alpha$ -  
463 pinene : Product and SOA formation. *Atmos. Environ.* 40, 116–127. <https://doi.org/10.1016/j.atmosenv.2005.09.093>,  
464 2006.

465 Sun, Y., Zhang, Q., Schwab, J.J., Yang, T., Ng, N.L., Demerjian, K.L.: Factor analysis of combined organic and inorganic  
466 aerosol mass spectra from high resolution aerosol mass spectrometer measurements. *Atmos. Chem. Phys.* 12, 8537–8551.  
467 <https://doi.org/10.5194/acp-12-8537-2012>, 2012.

468 Teng, A.P., Crounse, J.D., Lee, L., St. Clair, J.M., Cohen, R.C., Wennberg, P.O.: Hydroxy nitrate production in the OH-  
469 initiated oxidation of alkenes. *Atmos. Chem. Phys.* 139, 5367-5377. <https://doi.org/10.5194/acp-15-4297-2015>, 2015.

470 Teng, A.P., Crounse, J.D., Wennberg, P.O.: Isoprene Peroxy Radical Dynamics. *J. Am. Chem. Soc.* 15, 4297-4316.  
471 <https://doi.org/10.1021/jacs.6b12838>, 2017.

472 Wang, H.; Lu, K.; Chen, X.; Zhu, Q.; Chen, Q.; Guo, S.; Jiang, M.; Li, X.; Shang, D.; Tan, Z.; Wu, Y.; Wu, Z.; Zou, Q.; Zheng,  
473 Y.; Zeng, L.; Zhu, T.; Hu, M.; Zhang, Y.: High N<sub>2</sub>O<sub>5</sub> Concentrations Observed in Urban Beijing: Implications of a Large  
474 Nitrate Formation Pathway. *Environmental Science & Technology Letters*, 4, (10), 416-420.  
475 <https://doi.10.1021/acs.estlett.7b00341>, 2018.

476 Wang, M.; Zeng, L.; Lu, S.; Shao, M.; Liu, X.; Yu, X.; Chen, W.; Yuan, B.; Zhang, Q.; Hu, M.; Zhang, Z.: Development and  
477 validation of a cryogen-free automatic gas chromatograph system (GC-MS/FID) for online measurements of volatile  
478 organic compounds, 6, (23), 9424-9434. *Analytical Methods*, <https://doi.10.1039/C4AY01855A>, 2014.

479 Xu, L., Guo, H., Boyd, C.M., Klein, M., Bougiatioti, A., Cerully, K.M., Hite, J.R., Isaacman-VanWertz, G., Kreisberg, N.M.,  
480 Knotte, C., Olson, K., Koss, A., Goldstein, A.H., Hering, S. V., de Gouw, J., Baumann, K., Lee, S.-H., Nenes, A., Weber,  
481 R.J., Ng, N.L.: Effects of anthropogenic emissions on aerosol formation from isoprene and monoterpenes in the  
482 southeastern United States. *Proc. Natl. Acad. Sci.* 112, 37-42. <https://doi.org/10.1073/pnas.1417609112>, 2015a.

483 Xu, L., Suresh, S., Guo, H., Weber, R.J., Ng, N.L.: Aerosol characterization over the southeastern United States using high-  
484 resolution aerosol mass spectrometry: Spatial and seasonal variation of aerosol composition and sources with a focus on  
485 organic nitrates. *Atmos. Chem. Phys.* 15, 7307-7336. <https://doi.org/10.5194/acp-15-7307-2015>, 2015b.

486 Xu, W., Sun, Y., Wang, Q., Du, W., Zhao, J., Ge, X., Han, T., Zhang, Y., Zhou, W., Li, J., Fu, P., Wang, Z., Worsnop, D.R.:  
487 Seasonal Characterization of Organic Nitrogen in Atmospheric Aerosols Using High Resolution Aerosol Mass  
488 Spectrometry in Beijing, China. *ACS Earth Sp. Chem.* 1, 673–682. <https://doi.org/10.1021/acsearthspacechem.7b00106>,  
489 2017.

490 Yan, C., Nie, W., Äijälä, M., Rissanen, M.P., Canagaratna, M.R., Massoli, P., Junninen, H., Jokinen, T., Sarnela, N., Häme,  
491 S.A.K., Schobesberger, S., Canonaco, F., Yao, L., Prévôt, A.S.H., Petäjä, T., Kulmala, M., Sipilä, M., Worsnop, D.R.,  
492 Ehn, M.: Source characterization of highly oxidized multifunctional compounds in a boreal forest environment using  
493 positive matrix factorization. *Atmos. Chem. Phys.* 16, 12715-12731. <https://doi.org/10.5194/acp-16-12715-2016>, 2016.

494 Yuan, B., Hu, W. W., Shao, M., Wang, M., Chen, W. T., Lu, S. H., Zeng, L. M., and Hu, M.: VOC emissions, evolutions and  
495 contributions to SOA formation at a receptor site in eastern China, *Atmos. Chem. Phys.*, 13, 8815-8832,  
496 <https://doi.org/10.5194/acp-13-8815-2013>, 2013.

497 Zhang, Q., Jimenez, J.L., Canagaratna, M.R., Ulbrich, I.M., Ng, N.L., Worsnop, D.R., Sun, Y.: Understanding atmospheric  
498 organic aerosols via factor analysis of aerosol mass spectrometry: A review. *Anal. Bioanal. Chem.* 401, 3045-3067.  
499 <https://doi.org/10.1007/s00216-011-5355-y>, 2011.

500 Zhang, Y.H., Su, H., Zhong, L.J., Cheng, Y.F., Zeng, L.M., Wang, X.S., Xiang, Y.R., Wang, J.L., Gao, D.F., Shao, M., Fan,  
501 S.J., Liu, S.C.: Regional ozone pollution and observation-based approach for analyzing ozone-precursor relationship  
502 during the PRIDE-PRD2004 campaign. *Atmos. Environ.* 42, 6203-6218. <https://doi.org/10.1016/j.atmosenv.2008.05.002>,  
503 2008.

504 Zhu, B., Han, Y., Wang, C., Huang, X. F., Xia, S. Y., Niu, Y. B., Yin, Z. X., He, L.Y. :Understanding primary and secondary  
505 sources of ambient oxygenated volatile organic compounds in Shenzhen utilizing photochemical age-based  
506 parameterization method. *Journal of Environmental Sciences*, 75, 105-114. <https://doi.org/10.1016/j.jes.2018.03.008>,  
507 2019.

508 Zhu, Q., He, L.Y., Huang, X.F., Cao, L.M., Gong, Z.H., Wang, C., Zhuang, X., Hu, M.: Atmospheric aerosol compositions  
509 and sources at two national background sites in northern and southern China. *Atmos. Chem. Phys.* 16, 10283-10297.  
510 <https://doi.org/10.5194/acp-16-10283-2016>, 2016.

511 Zhu, Q., Huang, X.-F., Cao, L.-M., Wei, L.-T., Zhang, B., He, L.-Y., Elser, M., Canonaco, F., Slowik, J. G., Bozzetti, C., El-  
512 Haddad, I., and Prévôt, A. S. H.: Improved source apportionment of organic aerosols in complex urban air pollution using  
513 the multilinear engine (ME-2), *Atmos. Meas. Tech.*, 11, 1049-1060. <https://doi.org/10.5194/amt-11-1049-2018>, 2018.